ELSEVIER

Computational Materials Science 20 (2001) 57–65

COMPUTATIONAL MATERIALS SCIENCE

www.elsevier.com/locate/commatsci

A density functional study of small Ni_xSn clusters with $x = 1$–4

M. Finetti [a], E.E. Ottavianelli [a], R. Pis Diez [b,*], A.H. Jubert [b]

[a] *CIUNSa, Departamento de Química, Facultad de Ciencias Exactas, Universidad Nacional de Salta, Av. Bolivia 5150, 4400 Salta, Argentina*

[b] *CEQUINOR, Centro de Química Inorgánica (CONICET, UNLP), Departamento de Química, Facultad de Ciencias Exactas, UNLP C.C. 962, 1900 La Plata, Argentina*

Received 8 May 2000; accepted 21 June 2000

Abstract

Results of a systematic study of the geometry, electronic structure, magnetic, and vibrational properties of small Ni_xSn clusters, with $x = 1$–4, within the framework of the density functional theory are presented in this work. Population analyses are used to investigate the effect of tin on the nickel atoms towards an understanding of the changes in the catalytic behavior observed in the bimetallic system when it is compared with pure nickel.

Keywords: Ni–Sn cluster; Bimetallic clusters; Density functional theory

1. Introduction

Bimetallic catalysts involving tin and late transition metals are useful industrial catalysts for various hydrocarbon reactions. A significant amount of systematic studies on the deposition of tin on the (1 1 1) and (1 0 0) nickel surfaces have been conducted by several authors [1–4] showing the actual importance of this bimetallic system.

The formation of surface alloys seems to be very important in the chemical behavior of the bimetallic catalyst. The growth of metals on metals in a controlled manner provides tremendous opportunities for preparing ordered surface alloys, overlayers and superlattices with desired catalytic, non-corrosive and magnetic properties. Many studies of metal deposition have been concerned with the growth and structure of overlayers. For the time being more and more systems have been explored which show the formation of ordered surface alloys (see [3] and references therein). The bimetallic surfaces prepared by this approach have a unique reactivity which leads to considerable insight into the molecular details of how adsorbates bond and react at these surfaces [3].

Surface alloy formation is characterized by the intermixing of two metal components on the topmost atomic plane. Usually, alloy formation is expected if the constituent metals have similar metallic sizes and tend to form miscible solutions over a wide range of compositions. If the constituents have a dissimilar size but tend to form intermetallic compounds (e.g., Ni–Sn), then a nucleated intermetallic phase is formed on the surface.

* Corresponding author. Fax: +54-221-4259485.

E-mail address: pis_diez@dalton.quimica.unlp.edu.ar (R. Pis Diez).

0927-0256/01/$ - see front matter
PII: S0927-0256(00)00125-7

As far as we know there are neither experimental nor theoretical studies on Ni–Sn clusters. Clusters are useful as models for surfaces, and as such they have been used in the analysis of surface processes from a theoretical point of view [5]. It is believed that a systematic study of Ni–Sn clusters will shed some light into the electronic, magnetic and geometrical properties of a variety of surface sites of the bimetallic catalyst as well as into the nature of the surface alloy formed by the two metals.

A systematic study of Ni_xSn clusters, with $x = 1$–4, within the local and gradient-corrected density functional approximation is accomplished in the present work. Structural, electronic, magnetic, and vibrational properties of the stable conformers are also reported. The variation of the atomic charges and atom-like electron populations with the cluster size are also considered and discussed in relation to the potential catalytic activity of clusters.

2. Computational details

Density functional theory (DFT) calculations within the local spin density approximation (LSDA) [6–8] are performed on small Ni–Sn clusters using the Amsterdam density functional (ADF) package [9,10]. This code is based on Slater-type orbitals (STO) instead of the usual Gaussian-type functions. Furthermore, a set of auxiliary STOs are available to fit the electronic density in order to get a faster evaluation of the Coulomb potential.

The local correlation functional due to Vosko et al. [11] is used.

The triple-zeta basis set of STOs available as set IV in the package is used. This basis set does not include polarization functions. The frozen core approximation up to the 3p and 4p (included) orbitals are utilized for Ni and Sn, respectively.

The geometries and spin multiplicities of the Ni_xSn clusters, with $x = 1$–4, are optimized with the default convergence thresholds, i.e., 10^{-3} a.u. for the energy, 10^{-2} a.u. for the gradients, and 10^{-6} for the self-consistent cycle. The integration accuracy parameter is also set to its default value of 4.0 (see [12] for details about the numerical integration technique). Several symmetries are considered for each cluster and several different starting geometries are considered for each symmetry (see the next section for details). The optimizations are symmetry-constrained in all cases unless otherwise explicitly stated.

Frequency calculations are carried out on the optimized geometries to verify that these are the true minima on the potential surface of the corresponding cluster. If, on the other hand, the conformer is a saddle point then the imaginary modes are used to distort the system towards a true minimum. Frequency calculations are performed using default convergence and accuracy thresholds, i.e., 10^{-3} a.u. for the energy, 10^{-2} a.u. for the gradients, and 10^{-6} for the self-consistent cycle, and 6.0 for the integration accuracy parameter.

Density-gradient corrections are applied self-consistently to the LSDA geometries to achieve a better description of binding energies. The generalized gradient approximation (GGA) [13,14] is used to this end.

The electron smearing technique is used to remedy some convergence problems.

3. Results and discussion

The ground state of the Sn atom was found to be ^3P ($5s^25p^2$) in agreement with experimental data [15]. Table 1 shows our results for the different atomic states of tin as well as ionization potential values and their comparison with experimental data.

Table 1
Energy of different atomic states of Sn. The values are given in eV and the ground state is taken as the reference value. The experimental values are weighted averages over the J components

Atomic state	This work	Experimental[a]
^1D ($5s^25p^2$)	0.52 (0.64)[b]	0.76
^3P ($5s^25p^2$)	0.00	0.00
^5S ($5s^15p^3$)	4.56 (4.30)[b]	–
Ionization potential	7.50 (7.43)[b]	7.34

[a] Ref. [15].
[b] GGA values are given in parenthesis.

Prior calculations performed by some of us on nickel clusters include the complete characterization of the atomic states [16,17].

The binding energies reported throughout this work are evaluated using the calculated atomic ground state energies mentioned above as the reference values.

Tin dimer was mainly studied to validate the methodology to be used in this work. A $^3\Sigma_g^-$ state was found to be the ground state of Sn_2 in agreement with other theoretical results [18–21]. The valence electronic configuration at the LSDA level is

$$1\delta_g^4\ 1\delta_u^4\ 1\sigma_g^2\ 1\pi_u^4\ 1\pi_g^4\ 1\sigma_u^2\ 2\sigma_g^2\ 2\sigma_u^2\ 2\pi_u^2\ 3\sigma_g^2$$

Table 2 lists several calculated properties for the tin dimer as well as other theoretical and experimental results. It can be seen from the last table that a variety of theoretical methods, such as SCF/RCI calculations with and without spin-orbit effects [18,19], total-energy pseudopotential calculations within the LDA formalism [20], and frozen-core LDA and GGA calculations using double-zeta numerical basis sets [21], predict a bond length and a vibrational frequency in very good agreement with experimental values [22–24]. The experimental binding energy is reported to be 0.95 eV/at. [23]. The results obtained in [18–20] are in very good agreement with the experimental values though the multiplicity of the dimer ground state is not mentioned explicitly by Wang et al. [20]. On the other hand, the results reported in [21] and the results found in this work are very similar and quite higher than the experimental one [23], though GGA values present an important improvement over LDA ones. It must be emphasized that both methods use the frozen-core approximation up to the 3d [21] and 4p orbitals, respectively. This means that the valence space is sufficiently large in both cases. Although the error source in the binding energy is not clear at all, it could be attributed to a basis set effect, that is, pseudopotentials versus frozen-core approximation. In any case, the binding energies reported in this work should be considered as an upper limit of the yet unknown experimental energies.

3.1. NiSn

A $^1\Sigma^+$ state was found to be the ground state of NiSn. The valence electronic configuration is

$$1\delta^4\ 1\pi^4\ 1\sigma^2\ 2\sigma^2\ 3\sigma^2\ 2\pi^4\ 4\sigma^2\ 2\delta^4$$

The energies of the ground state and some low-lying excited states as well as other calculated properties of NiSn are shown in Table 3.

3.2. Ni_2Sn

The starting symmetries studied for Ni_2Sn were the $D_{\infty h}$ and $C_{\infty v}$ linear structures and the C_{2v} angular structure.

Table 2
Comparison of bond length (r, in Å), binding energy (BE, in eV/at.), and vibrational frequency (ω_e, in cm^{-1}) of the ground state of Sn_2 calculated in this work with other theoretical calculations and experimental results. Binding energies of low-lying excited states of Sn_2 calculated in this work are also shown. S is the total electronic spin

	S	State	r	BE	ω_e
SCF/RCI [18,19]		$^3\Sigma_g^-$	2.76	0.93	197
TE PS-LDA [20]		–	2.79	1.05	–
FC-LDA [21]		$^3\Sigma_g^-$	2.78 (2.94)[a]	1.53 (1.25)[a]	191 (166)[a]
	0			1.22	
This work	1	$^3\Sigma_g^-$	2.79	1.51 (1.27)[a]	186
	2			0.93	
Experimental		–	2.75[b]	0.95[c]	190[d]

[a] GGA value in parentheses.
[b] Ref. [22].
[c] Ref. [23].
[d] Ref. [24].

Table 3
Binding energies (BE, in eV/at.) of the ground state and some low-lying excited states of NiSn. The bond length (r, in Å) and vibrational frequency (ω_e, in cm^{-1}) of the ground state are also shown. S is the total electronic spin

S	State	BE	r	ω_e
0	$^1\Sigma^+$	1.84 (1.52)[a]	2.296	314
1		1.43		
2		0.82		

[a] GGA value in parentheses.

The ground state of the $D_{\infty h}$ conformer was found to be $^1\Sigma_g^+$. The vibrational analysis led to a set of real frequencies indicating that the conformer is a true minimum on the potential energy surface of Ni_2Sn. Its valence electronic configuration is

$$1\sigma_g^2\ 1\delta_g^4\ 1\pi_g^4\ 2\sigma_g^2\ 1\sigma_u^2\ 1\pi_u^4\ 2\pi_g^4\ 3\sigma_g^2\ 2\sigma_u^2\ 2\delta_g^4\ 1\delta_u^4$$

The ground state for the $C_{\infty v}$ structure was found to be a $^3\Delta$. One imaginary frequency along the Π mode suggested that the asymmetric conformer is a saddle point on the potential energy surface of Ni_2Sn. Unfortunately, no convergence was accomplished when the distortion along this mode was investigated.

A $^1A_1$ state was found to be the ground state for the C_{2v} symmetry. The vibrational analysis performed on this structure yielded only real frequencies indicating that it is a true minimum. The valence electronic configuration of the conformer is

$$1a_1^2\ 1a_2^2\ 1b_1^2\ 1b_2^2\ 2a_1^2\ 3a_1^2\ 4a_1^2\ 5a_1^2\ 2b_1^2\ 2b_2^2\ 6a_1^2\ 3b_1^2\ 3b_2^2\ 7a_1^2\ 2a_2^2\ 4b_2^2\ 3a_2^2$$

Table 4 summarizes the energies of the ground state and some low-lying excited states of the Ni_2Sn trimer in the different symmetries studied as well as other calculated properties of this system. It can be seen from this table that the angular conformer is considerably more stable than the linear one. Note also that there is an important increase in the Ni–Sn bond length as a consequence of the molecular bending. Finally, it is worth mentioning that the large difference between the smaller frequencies of the $D_{\infty h}$ $^1\Sigma_g^+$ and C_{2v} $^1A_1$ states calculated in this work could help future experimental measures to elucidate the nature of the ground state of Ni_2Sn.

3.3. Ni_3Sn

The starting symmetries studied for Ni_3Sn were the D_{3h} planar structure and the C_{3v} pyramidal structure.

The ground state of the D_{3h} conformer was found to be $^3E''$. The vibrational analysis performed on this structure led to an imaginary frequency along the E′ mode in agreement with what

Table 4
Binding energies (BE, in eV/at.) of the ground states and some low-lying excited states of Ni_2Sn in different symmetries. Geometrical parameters (r, in Å; θ, the apex angle, in degrees) and vibrational frequencies (ω_e, in cm^{-1}) of the corresponding stable ground states are also shown. S is the total electronic spin

Symmetry state	S	BE	r, θ	ω_e[a]
$D_{\infty h}$ $-^1\Sigma_g^+$	0	2.15 (1.75)[b]	2.279,–	58 (π_u^+), 262 (σ_g^+), 364 (σ_u^+)
	1	1.89		
	2	1.54		
$C_{\infty v}$[c]	0	1.76		
	1	1.82		
	2	1.62		
C_{2v} $-^1A_1$	0	2.48 (2.03)[b]	2.407, 54.3	222 (b_2), 285 (a_1), 335 (a_1)
	1	2.46		
	2	2.09		

[a] Symmetry assignment of frequencies is given in parentheses.
[b] GGA values in parentheses.
[c] This symmetry does not present stable conformers.

is expected on the basis of the Jahn–Teller theorem [25]. Unfortunately, distortion along this mode could not be carried out due to convergence problems.

A ^{3}E state was found to be the ground state for the C_{3v} structure. The vibrational analysis yielded six real frequencies. This fact is very surprising since the degenerate nature of the electronic state allows us to anticipate first-order Jahn–Teller deformations [25]. To solve this controversy, a subsequent geometric optimization was performed turning off the use of symmetry. The new and rather distorted structure is characterized by a triplet ground state ^{3}A. The vibrational analysis also led to a set of real frequencies indicating that the conformer is a true minimum on the potential energy surface of Ni_3Sn. Note that the valence electronic configuration is not reported in this case since there is only one irreducible representation for the C_1 point group.

Binding energy values of the ground states and some low-lying excited states of the Ni_3Sn conformers in different symmetries are shown in Table 5. Other calculated properties of the stable conformer are also summarized in this table. Fig. 1 shows the main geometric parameters of the stable conformer.

Table 5
Binding energies (BE, in eV/at.) of the ground states and some low-lying excited states of Ni_3Sn in different symmetries. Vibrational frequencies (ω_e, in cm^{-1}) of the corresponding stable ground states are also shown. S is the total electronic spin

Symmetry state	S	BE	ω_e
C_1–^{3}A	0	2.82	
	1	2.87	146, 173, 212,
		(2.38)[a]	227, 332, 351
	2	2.81	
D_{3h}[b]	0	2.09	
	1	2.17	
	2	1.83	
C_{3v}[b]	0	2.82	
	1	2.87	
	2	2.81	

[a] GGE value in parenthesis.
[b] This symmetry does not present stable conformers.

3.4. Ni_4Sn

To simplify the study of Ni_4Sn clusters, two-dimensional (2D) and three-dimensional (3D) structures are discussed separately. Results are then presented as two different subsections.

3.4.1. 2D structures

The starting 2D symmetry was the D_{4h} planar square structure.

A ^3E_g electronic state was found to be the ground state for the square conformer. The vibrational analysis yielded three imaginary frequencies along the B_{2g}, E_u and A_{2u} modes. Distortions along these modes yielded a D_{2h} rectangular structure, a C_{2v} rectangular pyramid, and a C_{4v} square pyramid structure, respectively.

The D_{2h} conformer presented a ground state characterized by a $^3B_{3g}$ electronic state. The vib-

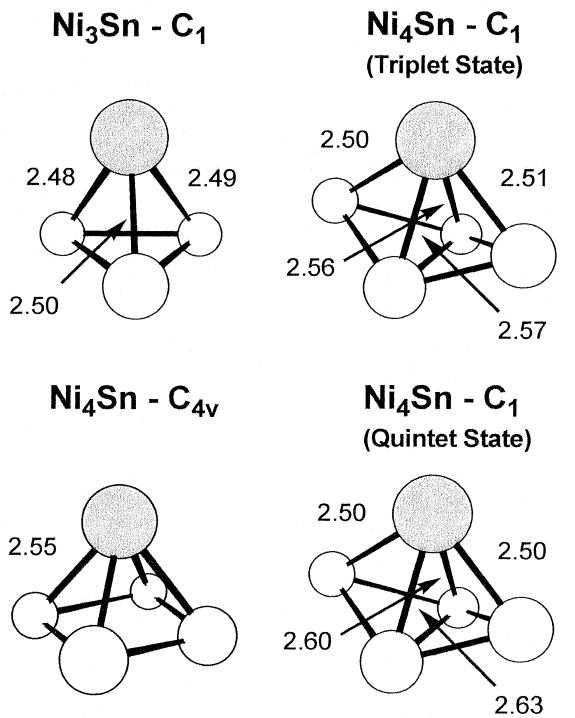

Fig. 1. Geometric parameters of stable Ni_3Sn and Ni_4Sn conformers. Bond lengths are in Å. White and gray circles are nickel and tin atoms, respectively.

rational analysis yielded two imaginary frequencies along the A_u and B_{3u} modes. Distortion along these two modes led to the same, non-symmetric conformer which will be discussed in the next subsection as it is a 3D structure.

The C_{2v} and C_{4v} structures found from distortion of the E_u and A_{2u} modes, respectively, will be discussed in the next subsection as these also are 3D conformers.

The binding energies of the ground states and some low-lying excited states of the 2D Ni_4Sn conformers in different symmetries are shown in Table 6.

Table 6
Binding energies (BE, in eV/at.) of the ground states and some low-lying excited states of Ni_4Sn in different symmetries. Vibrational frequencies (ω_e, in cm^{-1}) of the corresponding stable ground states are also shown. S is the total electronic spin

Symmetry state	S	BE	ω_e
D_{4h}[a]	0	2.23	
	1	2.29	
	2	2.11	
D^a_{2h}	0	2.58	
	1	2.61	
	2	2.54	
T^a_d	0	1.87	
	1	2.08	
	2	2.16	
	3	2.02	
C^a_{2v}	0	2.58	
	1	2.60	
	2	2.53	
C_1	0	3.02	
	1	3.09 (2.45)[b]	85, 124, 139, 187, 197, 213, 233, 282, 335
	2	3.11 (2.47)[b]	87, 119, 175, 177, 210, 217, 226, 301, 327
	3	2.75	
C_{4v}	0	2.96	
	1	3.02	
	2	3.08 (2.57)[b]	71(b_1), 146(e), 146(b_1), 192(a_1), 259(b_2), 277(e), 306(a_1)
	3	2.75	

[a] This symmetry does not present stable conformers.
[b] GGA values in parenthesis.

3.4.2. 3D structures

In the case of 3D structures, the starting symmetry was the T_d perfect tetrahedron.

A $^5T_1$ state characterizes the ground state of the tetrahedral structure. The vibrational analysis could not be accomplished due to convergence problems. However, it should be noted that the degenerate nature of the ground state allows us to anticipate the presence of first-order Jahn–Teller effects [25]. Thus, it is safe to say that the tetrahedral structure must be a saddle point on the potential energy surface of Ni_4Sn.

The ground state of the C_{2v} conformer found from distortion of the E_u mode of the D_{4h} structure mentioned in the last subsection was found to be $^3B_2$. The vibrational analysis yielded an imaginary frequency along the B_1 mode. Further distortion along this mode led to a non-symmetric, C_1 conformer that turned out to be a true minimum on the potential energy surface of Ni_4Sn after the vibrational analysis. The ground state of this conformer is found to be ^3A. This conformer is exactly the same as that obtained from distortion of the two imaginary modes of the D_{2h} structure mentioned in the last subsection.

To complete the study of the C_1 conformer, other electron spin multiplicities were considered. A quintet state, ^5A, was found to be stable after the vibrational analysis and, moreover, it turned out to be the lowest-energy conformer of Ni_4Sn.

The C_{4v} structure found from distortion of the A_{2u} mode of the D_{4h} conformer mentioned in the last subsection was also studied. A $^5B_1$ state was found to be the ground state. The vibrational analysis yielded a set of real frequencies indicating that the conformer is a true minimum on the potential energy surface of Ni_4Sn. Its valence electronic configuration is

$$1e^4\ 1a_1^2\ 1b_1^2\ 1b_2^2\ 2a_1^2\ 3a_1^2\ 2b_2^2\ 2e^4\ 4a_1^2\ 5a_1^2\ 3e^4\ 3b_2^2\ 4e^4$$
$$5e^4\ 6a_1^2\ 2b_1^2\ 6e^4\ 1a_2^2\ 3b_1^2\ 4b_1^1\ (\uparrow)\ 2a_2^1\ (\uparrow)\ 4b_1^2\ 7e^2(\uparrow)$$

The binding energies of the ground states and some low-lying excited states of the 3D Ni_4Sn conformers in different symmetries are shown in

Table 6. Other calculated properties of the stable conformers are also summarized in this table. Fig. 1 shows the relevant geometric parameters for the stable conformers.

Table 7 shows the atomic charges on every cluster calculated according to both the Mulliken analysis [26] and the Voronoi charge analysis. [1] The sp and d orbital populations on the nickel atoms, derived from the Mulliken analysis, are also shown in the table.

It can be seen that a charge transfer process takes place from tin to the nickel atoms for all the clusters studied in the present work. Moreover, it is noted for the bigger clusters that Voronoi charges are smaller for those nickel atoms which are more distant from the tin atom. The Mulliken charges do not evidence the same behavior as can be seen in the quintet state of the non-symmetric Ni_4Sn cluster.

On the other hand, it is also noted for the bigger clusters that the sp population shows a more pronounced increase of those nickel atoms being more distant from Sn. On the contrary, the d population reduces its value for these atoms. It should be recalled that an isolated nickel atom is charaterized by a d^9s^1 configuration according to the LSDA [16].

It is interesting at this point to stress that bimetallic catalysts such as Ni–Sn [27] and Pt–Sn [28] are less active than the corresponding monometallic systems for the H–H bond activation. From a mechanistic point of view, the H–H activation by monometallic systems occurs as a two-step process [29]. Firstly, the occupied σ molecular orbital of dihydrogen donates charge to the empty s atom-like orbital of the metal centre. Then, an occupied d atom-like orbital of the metal centre donates charge into the empty σ^* molecular orbital of dihydrogen. Both processes lead to an effective H–H bond weakening, thus, facilitating H_2 activation. It is argued, on the other hand, that a p atom-like orbital of Sn interacts with the d atom-like orbital of Ni (Pt), thus, reducing the charge transfer to the H_2 σ^* molecular orbital, hence the H–H bond activation by the bimetallic catalyst [29]. It is unclear yet if Sn atoms are also responsible for geometric effects yielding a further decrease in the H–H bond activation by the bimetallic system.

Assuming the validity of the above electronic mechanism for the clusters studied in the present work, it is clear that the σ donation from dihydrogen to nickel should decrease with an increase in the sp population of nickel atoms. On the other hand, the donation from nickel to the empty σ^* molecular orbital of dihydrogen should also decrease with a decrease in the d population of nickel atoms. Thus, it can be seen that those nickel atoms located more distantly from the tin atom should be less active to capture and dissociate dihydrogen than those nickel atoms being nearer tin since these atoms show a more pronounced increase in the sp population and a decrease in the d population.

It would be also interesting to further investigate if the ability of those nickel atoms near tin to capture dihydrogen is reduced by additional geometric effects attributed to the metal belonging to group 14. Future work involving large Ni–Sn clusters is being performed to investigate more deeply into those facts related to the possible catalytic activity of clusters.

4. Conclusions

A density functional study of small Ni_xSn clusters, $x = 1$–4, was performed in this work.

A stable conformer was found for NiSn. Two Ni_2Sn conformers, a linear one and a bent one, were found to be stable. An almost pyramidal Ni_3Sn conformer turned out to be a minimum. Three stable conformers were found for Ni_4Sn, one with a pyramidal geometry and two in a non-symmetric structure. Geometric parameters, electronic configurations, magnetic moments, and vibrational frequencies are reported for all of them to completely characterize their states.

A digression is made concerning the experimental findings on the decrease of the activity of

[1] The Voronoi charge analysis is based on assigning the density in a given point in space to the nearest atom. Then, the atomic charges are obtained by means of a numerical integration scheme of the charge density on each atom.

Table 7
Atomic charges (Q) calculated according the Voronoi analysis and the Mulliken analysis (in parentheses), both in $|e| \times 10^3$. sp and d populations on the nickel atoms obtained from the Mulliken analysis are also shown. The subscripts used to label the nickel atoms indicate proximity to Sn, the lower the subscript, the nearer the nickel atom is to tin

	Sn	Ni_1			Ni_2			Ni_3			Ni_4		
	Q	Q	sp	d	Q	sp	d	Q	sp	d	Q	sp	d
NiSn	404 (214)	−404 (−214)	1.16	9.05									
Ni_2Sn[a]	690 (201)	−345 (−100)	0.87	9.23									
Ni_2Sn[b]	443 (278)	−221 (−139)	1.08	9.06									
Ni_3Sn	435 (295)	−154 (−102)	1.14	8.97	−97 (−75)	1.07	9.00	−185 (−120)	1.17	8.95			
Ni_4Sn[c]	506 (356)	−126 (−89)	1.17	8.92									
Ni_4Sn[d]	523 (378)	−175 (−102)	1.06	9.04	−172 (−101)	1.07	9.03	−92 (−89)	1.13	8.96	−85 (−86)	1.13	8.96
Ni_4Sn[d]	494 (361)	−145 (−88)	1.12	8.97	−146 (−90)	1.12	8.97	−107 (−96)	1.23	8.87	−97 (−86)	1.22	8.87

[a] $D_{\infty h}$ symmetry.
[b] C_{2v} symmetry.
[c] C_{4v} symmetry.
[d] C_1 symmetry, triplet state.
[d] C_1 symmetry, quintet state.

bimetallic Ni–Sn catalyst with respect to pure Ni against the capture and dissociation of dihydrogen. The present results suggest that tin is responsible for the electronic effects on the farther nickel atoms through a decrease in the strength of the charge transfer process associated to the H–H bond activation in H_2.

Additional calculations must be performed to elucidate possible geometric effects associated to Sn on the nearer nickel atoms as well as the selectivity showed by the bimetallic system.

Acknowledgements

The authors acknowledge ANPCyT, Argentina, for the financial support under grant PICT97 06-00000-01612. They also thank CIUNSa for the partial financial support. EEO, RPD and AHJ are members of the Scientific Research Carrers of CONICET, and CICPBA, Argentina, respectively.

References

[1] S.H. Overbury, D.R. Mullins, M.F. Paffett, B.E. Koel, Surf. Sci. 254 (1991) 45.
[2] S.H. Overbury, Y. Ku, Phys. Rev. B 46 (1992) 7868.
[3] Y.D. Li, Q. Hang, B.E. Koel, Phys. Rev. B 49 (1993) 2813.
[4] C. Xu, B.E. Koel, Surf. Sci. 327 (1995) 38.
[5] G. Pacchioni, P.S. Bagus, F. Parmigiani, Clusters Models for Surface and Bulk Phenomena, Plenum Press, New York, 1992.
[6] P. Hohenberg, W. Kohn, Phys. Rev. B 136 (1964) 864.
[7] W. Kohn, L.J. Sham, Phys. Rev. B 140 (1965) 1133.
[8] R.G. Parr, W. Yang, Density Functional Theory of Atoms and Molecules, Oxford University Press, New York, 1989.
[9] ADF 1999, E.J. Baerends, A. Bérces, C. Bo, P.M. Boerrigter, L. Cavallo, L. Deng, R.M. Dickson, D.E. Ellis, L. Fan, T.H. Fischer, C. Fonseca Guerra, S.J.A. van Gisbergen, J.A. Groeneveld, O.V. Gritsenko, F.E. Harris, P. van den Hoek, H. Jacobsen, G. van Kessel, F. Kootstra, E. van Lenthe, V.P. Osinga, P.H.T. Philipsen, D. Post, C.C. Pye, W. Ravenek, P. Ros, P.R.T. Schipper, G. Schreckenbach, J.G. Snijders, M. Sola, D. Swerhone, G. te Velde, P. Vernooijs, L. Versluis, O. Visser, E. van Wezenbeek, G. Wiesenekker, S.K. Wolff, T.K. Woo, T. Ziegler.
[10] C.F. Guerra, J.G. Snijders, G. te Velde, E.J. Baerends, Theoret. Chem. Acc. 99 (1998) 391.
[11] S.H. Vosko, L. Wilk, M. Nusair, Can. J. Phys. 58 (1980) 1200.
[12] G. te Velde, E.J. Baerends, J. Comp. Phys. 99 (1992) 84.
[13] J.P. Perdew, in: P. Ziesche, H. Eschring (Eds.), Electronic Structure of Solids '91, Akademie, Berlin, 1991.
[14] J.P. Perdew, J.A. Chevary, S.H. Vosko, K.A. Jackson, M.R. Pederson, D.J. Singh, C. Fiolhais, Phys. Rev. B 46 (1992) 6671.
[15] C.E. Moore, Atomic Energy Levels, Natl. Bur. Stand., Circ. 467 (1952).
[16] M.C. Michelini, R. Pis Diez, A.H. Jubert, Int. J. Quantum Chem. 70 (1998) 693.
[17] M.C. Michelini, R. Pis Diez, A.H. Jubert, J. Mol. Struct. 490 (1999) 181.
[18] K. Balasubramanian, K.S. Pitzer, J. Chem. Phys. 78 (1983) 321.
[19] K. Balasubramanian, K.S. Pitzer, Erratum, J. Chem. Phys. 80 (1984) 592.
[20] B. Wang, L.M. Molina, M.J. López, A. Rubio, J.A. Alonso, M.J. Stott, Ann. Phys. 7 (1998) 107.
[21] P. Jackson, I.G. Dance, K.J. Fischer, G.D. Willet, G.E. Gadd, Int. J. Mass Spectrom. Ion Process. 157/158 (1996) 329.
[22] V.E. Bondybey, M.C. Heaven, T.A. Miller, J. Chem. Phys. 78 (1983) 3593.
[23] K. Pak, M.F. Cai, T.P. Dzugan, V.E. Bondybey, Faraday Discuss. Chem. Soc. 86 (1988) 153.
[24] V.E. Bondybey, J.H. English, J. Chem. Phys. 76 (1982) 2165.
[25] I.B. Bersuker, The Jahn–Teller Effect and Vibronic Interactions in Modern Chemistry, Plenum Press, New York, 1984.
[26] R.S. Mulliken, J. Chem. Phys. 23 (1955) 1833.
[27] G.F. Santori, Ph.D. Thesis, Departamento de Ingeniería Química, Facultad de Ingeniería, Universidad Nacional de La Plata, March 2000.
[28] R.D. Cortright, J.A. Dumesic, Appl. Catal. A 129 (1995) 101.
[29] G. Aguilar-Ríos, M. Valenzuela, P. Salas, H. Armendáriz, P. Bosch, G. Del Toro, R. Silva, V. Bertín, S. Castillo, A. Ramírez-Solís, I. Schifter, Appl. Catal. A 127 (1995) 65.